PHYSICAL REVIEW E VOLUME 51, NUMBER 1 JANUARY 1995

# X-ray reflectivity study of interface roughness, structure, and morphology of alignment layers and thin liquid crystal films

Brian Cull, Yushan Shi, and Satyendra Kumar
*Department of Physics and Liquid Crystal Institute, Kent State University, Kent, Ohio 44242*

Raymond Shih and J. Mann
*Department of Chemical Engineering, Case Western Reserve University, Cleveland, Ohio 44106*
(Received 1 August 1994)

We report results of x-ray reflectivity studies of thin conducting films, organic alignment layers, and liquid crystal films on flat glass substrates. An understanding of these films is important for liquid crystal science and technology. Specular reflectivities of conducting layers of indium tin oxide, organic overlayers of lecithin, 12-8(poly)diacetylene polymerized with linearly polarized uv light, and spin-coated diheptylazoxy benzene films were measured. The evolution of surface roughness of soda-lime glass substrates as a function of chemical etching time was also studied. Using theoretical models based on the Fourier transform of electron density gradients and the matrix formalism of x-ray optics, we quantitatively determined film thickness, layer spacing, electron density, and rms surface roughness and height-height correlations.

PACS number(s): 61.10.−i, 68.55.Jk, 78.20.Ci

## I. INTRODUCTION

Study of surfaces and thin liquid crystal films is important in understanding the properties of liquid crystals under confinement and the effect of surface roughness on their phase behavior. Quantitative determination of film structure, surface roughness, its chemical nature, and anchoring of liquid crystal molecules is also essential for building high-quality electro-optical devices. Information about surface agents that provide homeotropic (e.g., lecithin) or homogeneous (e.g., rubbed polyimide) alignment can be extracted by various techniques: molecular orientation from second harmonic generation [1], chemical composition of layers by x-ray photoelectron spectroscopy [2], topology by atomic force microscopy [3], and structure and phase transitions through x-ray scattering [4].

X-ray reflectivity [5] is a technique which has become popular in the past decade and is primarily based on high flux x-ray sources and improved x-ray instrumentation. X-ray reflectivity is a nondestructive probe of surface morphology and structure. It has the dual advantages of being able to measure small electron density variations as well as determine overall layer structure at surfaces and in thin films. Monolayer structure and roughness on a liquid surface [6] and layer-by-layer growth, for example, at the nematic–smectic-*A* phase transition [7] can be measured with high accuracy. The reflectivity technique has been used to probe layer fluctuations in thin smectic-*A* films [8] and interfacial roughness [9].

Using x-ray reflectivity, we were able to determine many important parameters, such as electron density and its modulation along the surface normal, film thickness, interfacial roughness, and surface morphology. We discovered several interesting phenomena of both scientific interest and technological importance. In this paper, we report the results of x-ray reflectivity studies of changes in the roughness of substrate surface as a result of chemical etching, thin conducting layers of indium tin oxide (ITO), alignment layers of egg lecithin, Langmuir-Blodgett films of linearly photopolymerized 12-8(poly)diacetylene (PDA), and thin liquid crystal films of diheptylazoxybenzene (D7AOB). We have quantitatively determined the electron density of the glass substrate and the exponents of surface roughness resulting from chemical etching by KOH-water solutions on a single substrate as a function of soaking time. The electron density and thickness of films of ITO were accurately determined, as well as the presence of a 1300 Å $SiO_2$ undercoating deposited by the manufacturer (Donnally) to prevent migration of alkali ions. Lecithin molecules formed stratified films on the surface of glass which resulted in specular reflectivity scans consisting of a coherent summation of Kiessig fringes arising from overall film thickness and Bragg peaks from internal layering. Anisotropy in surface morphology induced by photopolymerization using polarized uv light was observed for 12-8(poly)diacetylene Langmuir-Blodgett (LB) films. An adsorbed bilayer with crystalline order was observed at the film-substrate interface in D7AOB films which persisted $\sim 30\,^{\circ}$C above the nematic-isotropic bulk transition temperature.

## II. THEORETICAL BACKGROUND

X-ray diffraction has long been known to be one of the most powerful techniques available to probe the structure of condensed matter [10]. Because the scattering cross section of x rays in matter is small, only single scattering events need to be considered in conventional structural analysis, which makes the data interpretation

 ©1995 The American Physical Society

simple and straightforward by allowing the use of the kinematic treatment of x-ray scattering [11]. In this case, conservation of scattered intensity is not considered and the difference of x-ray refractive indices between the material and air is ignored.

The dynamical theory of x-ray scattering is a more rigorous treatment as it takes into account the interference between the incident and scattered waves [12]. In this case, the refractive index of x rays in matter plays an important role in describing optical effects and it is written as

$$n = 1 - \delta + i\beta = 1 - \frac{\lambda^2 r_0}{2\pi}\rho + i\frac{\lambda\mu}{4\pi}, \quad (1)$$

where $\lambda$ is the wavelength of x rays, $r_0$ the classical electron radius, $\rho$ the electron density of matter, and $\mu$ the mass absorption coefficient. The values of $\delta \sim 10^{-5}$ and $\beta \sim 10^{-7}$ for condensed matter are very small but measurable.

At an ideal interface, i.e., smooth and sharp, between two semi-infinite media (e.g., air and a dielectric), the propagation of x rays obeys Snell's law [12]. Because the value of $n$ is smaller than unity, total external reflection of x rays occurs at the dielectric surface for angles of incidence smaller than the critical angle, $\theta_c = \sqrt{2\delta}$, which directly depends on the electron density of the medium. Reflectivity ($R$) of a single interface as a function of the glancing incidence angle $\theta$, or x-ray momentum transfer $q = \frac{4\pi}{\lambda}\sin\theta$ along the surface normal, is given by the well-known Fresnel formula [13] and may be written

$$F(q) = |r|^2 = \left|\frac{q - \sqrt{q^2 - q_c^2}}{q + \sqrt{q^2 - q_c^2}}\right|^2, \quad (2)$$

where $r$ denotes the x-ray reflectance at the interface and $q_c$ is the critical momentum transfer vector corresponding to $\theta_c$. In this case, the exit angle of the reflected x-ray beam with respect to the surface is always the same as that of the incident beam.

A real interface, as shown in Fig. 1(a), always has some roughness associated with it, which generates diffuse scattering and reduces the specular reflectivity described in Eq. (2) for x-ray reflection. By assuming the interfacial roughness is self-affine [14] and due to a random distribution of atoms or molecules along the surface normal ($z$ axis) of an average interface, the loss of specular reflectivity as a function of $q_z$ can be accounted for by a Debye-Waller-like factor. X-ray specular reflectivity of a single rough surface can be written as

$$R(q_z)_{\text{spec}} = F(q_z)\exp[-q_z\sqrt{(q_z^2 - q_c{}^2)}\sigma^2], \quad (3)$$

where $\sigma$ is the rms value of surface roughness along the $z$ axis, i.e., the height distribution over a smooth average interface. The diffuse scattering can be written as a function of the normal component, $q_z$, and in-plane component, $q_x$, of the momentum transfer as [15]

$$R(q_x, q_z)_{\text{diff}} = CR(q_z)_{\text{spec}} \times \int_0^\infty \exp\left\{q_z^2\sigma^2 \exp\left[-\left(\frac{S}{\xi}\right)^{2h}\right]\right\} \times J_0(q_x S) S dS, \quad (4)$$

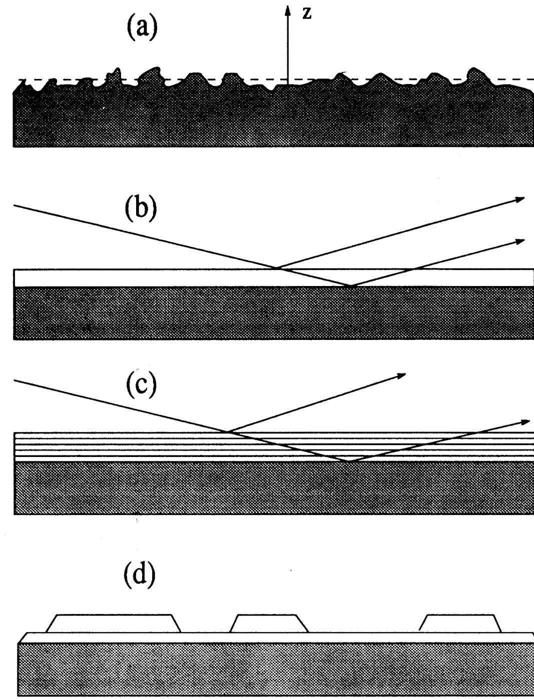


FIG. 1. Morphologies of various physical systems examined using x-ray reflectivity in this paper: (a) rough glass substrate having associated parameters electron density $\rho_s$, rms roughness $\sigma$, and roughness exponent $h$, (b) monolayer on solid substrate with film density $\rho_f$, film thickness $t$, and air-film and film-substrate interfacial roughnesses $\sigma_{1,2}$, (c) stratified film with layer spacing $d$, and (d) Stranski-Krastanov growth of clusters on top of thin film.

where $S$ is the in-plane coordinate in real space, $C$ is a proportionality constant, $h$ and $\xi$ are roughness exponents denoting the fractal dimension and cutoff length of height-height correlations, respectively, and $J_0(q_x S)$ is the zeroth-order Bessel function. The relation between the height-height correlation function and these roughness components can usually be written

$$g(S) = 2\sigma^2\left\{1 - \exp\left[-\left(\frac{S}{\xi}\right)^{2h}\right]\right\}. \quad (5)$$

The value of $h$ can vary from near 0, which indicates an extremely jagged rough surface, to near 1, which indicates a relatively smooth (i.e., slowly varying roughness) surface. The value of $\xi$ reflects a combined effect of the finite size on the interface and the coherence of the incidence beam. By simply substituting $x$ for $y$, the diffuse scattering $R(q_y, q_z)_{\text{diff}}$ may be studied.

When a uniform thin film is deposited on a substrate as shown in Fig. 1(b), two interfaces, i.e., the air-film and film-substrate interfaces, must be considered. To simplify the problem, we assume that the roughnesses at these interfaces are described by two independent parameters $\sigma_{af}$ and $\sigma_{fs}$ (i.e., uncorrelated roughness), so the x-ray specular reflectivity can be written as [13]

$$R(q_z) = \left| \frac{r_{af} + r_{fs}\exp(inq_z t)}{1 + r_{af} r_{fs}\exp(inq_z t)} \right|^2 , \quad (6)$$

where $t$ and $n$ are the thickness and x-ray refractive index of the film, and $r_{af}$ and $r_{fs}$ are the x-ray reflectances at the air-film and film-substrate interfaces, respectively. The subscripts $a$, $f$, and $s$ refer to air, film, and substrate, respectively. Even though in some cases, such as in our studies of adsorbed layers and LB films, the roughnesses at the two interfaces are actually found to be highly correlated as indicated by the diffuse scattering [16], Eq. (6) can still be used in data analysis by fixing the rms roughness $\sigma_{fs}$, which was determined *a priori* by independent measurement of the bare surface roughness. Interference of x rays reflected from the two interfaces produces Kiessig fringes [17], provided that the thickness of the film does not exceed the coherence length of the incident x-ray beam. The periodicity (spacing) of these fringes gives a highly accurate measurement of the film thickness. The amplitude of these fringes provides information on the electron density contrast between the film and substrate, and also on the uniformity and morphology of the thin film.

For a multilayer film, in which more than two interfaces are present, the matrix method of optics [13] has been used to describe the x-ray reflection. Each uniform thin sublayer of given thickness $t$ and refractive index $n$ can be assigned a characteristic matrix $M$ [18] such that

$$M = \begin{vmatrix} \cos(nq_z t/2) & -(i/p)\sin(nq_z t/2) \\ -ip\sin(nq_z t/2) & \cos(nq_z t/2) \end{vmatrix} , \quad (7)$$

where we define $p \equiv n\cos\theta$ for the film, where $\theta$ is the angle made by the incident beam wave vector measured from the substrate surface. The characteristic matrix $M_{\text{total}}$ for a multilayer film is simply a product of such matrices of single layers in sequential order from the top surface to the substrate. The reflectivity can be written as

$$R(q_z) = \left| \frac{(m_{00} + m_{01}p_s)p_a - (m_{10} + m_{11}p_s)}{(m_{00} + m_{01}p_s)p_a + (m_{10} + m_{11}p_s)} \right|^2 , \quad (8)$$

where $m_{ij}$ refers to the $ij$th element of the characteristic matrix $M_{\text{total}}$. This method allows easy modeling of the electron density variation along the surface normal. It is especially suitable where rough interfaces or electron density distributions vary independently from layer to layer. However, the disadvantage of the matrix method is that many parameters can be introduced which cannot be determined independent of some *a priori* knowledge of the system, e.g., known molecular arrangement resulting from regular deposition via the Langmuir-Blodgett method.

Under the Born approximation, a quasidynamical treatment of x-ray specular reflection from a surface with continuous electron density modulation along the surface normal can be derived for $q_z \gg q_c$ [18],

$$R(q_z) = \left| \frac{8\pi^2}{\lambda^2 q_z^2} \int_{-\infty}^{\infty} \frac{d\delta(z)}{dz} \exp(iq_z z)\, dz \right|^2 . \quad (9)$$

This formula indicates that $R(q)$ is sensitive to variation in electron density along the substrate normal. For a film comprised of sublayers such as a Langmuir-Blodgett film, each has the same form factor in the normal direction as shown in Fig. 1(c). An expression for $R$ can be obtained from Eq. (6) [19] for an even number of layers,

$$R(q_z) = \left(\frac{8\pi^2}{\lambda^2 q_z}\right)^2 \left[ \frac{(\delta_s - 2\delta_f)^2}{q_z^2} + \frac{4\delta_f(\delta_s - \delta_f)}{q_z^2}\cos^2\left(\frac{Nq_z d}{2}\right) + B^2 \frac{\sin^2(Nq_z d/2)}{\sin^2(q_z d/2)} + \frac{2B}{q_z}(2\delta_f - \delta_s)\frac{\sin^2(Nq_z d/2)}{\sin(q_z d/2)} \right] . \quad (10)$$

Here, $B$ is the bilayer form factor, $B = \int_{-d/2}^{d/2} [\delta(z) - \delta_f] \exp(iqz)\, dz$, $d$ is individual bilayer spacing, and $N$ is the number of bilayers in the film. The corresponding equation for an odd number of layers is [19]

$$R(q_z) = \left(\frac{8\pi^2}{\lambda^2 q_z}\right)^2 \left[ \frac{(\delta_s - 2\delta_f)^2}{q_z^2} + \frac{4\delta_f(\delta_s - \delta_f)}{q_z^2}\cos^2\left(\frac{(N+\frac{1}{2})q_z d}{2}\right) + B^2\frac{\sin^2(Nq_z d/2)}{\sin^2(q_z d/2)} + \frac{2B}{q_z}\frac{\sin(Nq_z d/2)}{\sin(q_z d/2)} \{(\delta_f - \delta_s)\sin[(N+1)q_z d/2] + \delta_f \sin(Nq_z d/2)\} \right] . \quad (11)$$

Even though the above two equations are specialized treatments of x-ray reflection, they provide physical insight into the origins of the interference observed. The first two terms of this expression describe the contribution from Fresnel scattering of the film, give rise to Kiessig fringes, and depend principally on the properties of the two interfaces. The third term is the Bragg contribution described in kinematical treatment of x-ray scattering and is determined entirely by the periodic structure of the bilayers. The last term represents an interesting coupling between the Fresnel and Bragg scatterings, which may result in a shift and modulation of the peaks. This coupling term, also determined by the coherence area of the incident x-ray beam, can provide useful information on the surface morphology of this system.

## III. EXPERIMENTAL SETUP

Reflectivity measurements were performed on a variety of physical systems, including bare substrate and several

different organic overlayers using the Cu $K\alpha$ line on a Rigaku 12 kW rotating anode with a pair of Si(1 1 1) single crystals as monochromator and analyzer. The direction normal to the sample surface defined the origin of angle $\omega$. The instrumental resolution was $\sim 2.6\times10^{-4}$ Å$^{-1}$ in the longitudinal direction and $\sim 5.2\times10^{-2}$ Å$^{-1}$ in the out-of-plane direction. A slit, 0.4 mm and 5.0 mm in horizontal and vertical directions, respectively, corresponding to the in-plane $w_{\rm in}$ and out-of-plane $w_{\rm out}$ widths was placed 135 mm in front of the sample to define the incident beam. The incident x rays were essentially uniformly distributed over the beam cross section in the scattering plane and symmetrically distributed out of the scattering plane. Samples, 51 mm $\times$ 51 mm, were mounted on a Huber two-circle goniometer in a custom-made oven on one of the vertical surfaces. The oven [Fig. 2(a)] consisted of two parallel plates separated by 30 mm, designed so as to eliminate a temperature gradient near the exposed surface. A Mylar window allowed x rays to pass through but helped in temperature stability. The oven was surrounded by thermally insulating ceramic foam. Temperature fluctuations were measured to be smaller than 0.01 K. The oven was purged with dry nitrogen when moisture-sensitive lecithin measurements were made.

Longitudinal scans [Fig. 2(b)] were conducted under the condition of specular reflectivity ($\omega=0$). Nonspecular longitudinal scans (performed at $\omega=\pm0.03°$ in most cases) were subtracted as diffuse scattering and the scattered intensity normalized with respect to the incident beam. To account for finite sample size, a footprint correction was applied by multiplying the reflected intensity for angle $\theta \leq \sin^{-1}(\frac{w_{\rm in}}{l})$ by the factor $(\frac{w_{\rm in}}{l\sin\theta})$, where $l$ is sample length.

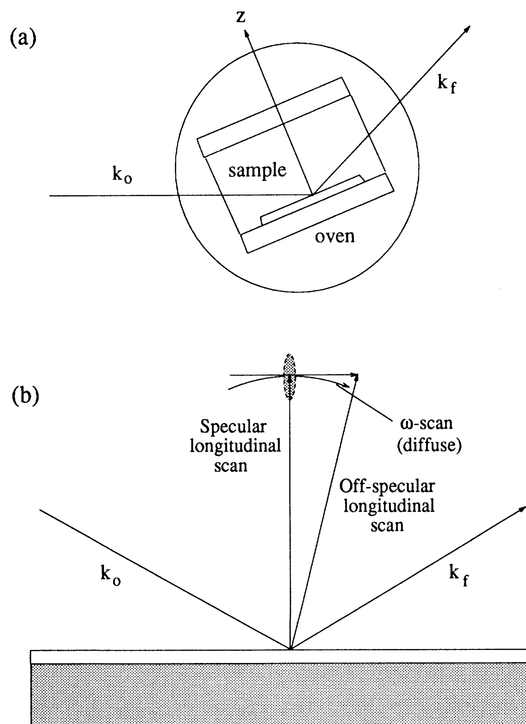


FIG. 2. (a) Sample orientation in oven with respect to incident and scattered wave vectors $k_0$ and $k_f$. (b) Scattering geometry showing orientation of momentum transfer vector in performing specular, off-specular, and diffuse scans.

## IV. SAMPLE PREPARATION

Rough surfaces of soda-lime glass plates were prepared by cleaning in a nitric acid bath (judged clean when distilled water formed a continuous film over the surface rather than aggregating to form droplets). The plates were then rinsed with acetone, and dried at 120 °C for 20 min and blown off with dry nitrogen to remove dust. These plates were then ultrasonicated in a 40% KOH-water solution for 0, 5, 8, and 12 h at 24 °C, followed by washing in distilled water to remove residues.

Alignment layers and organic films were prepared by dipping the substrate in a dilute solution or spin coating in a Class 100 clean room. Dipping was performed using a beaker with drainage tube and stopcock allowing control of the speed of flow of solution over the sample. The substrate was placed vertically within the beaker, and solution filled to the desired level. The solution was then drained at a rate of between 0.5 cm/s and 2.0 cm/s. Egg lecithin was deposited by dipping clean soda-lime glass plates in 0.2% and 2.0% lecithin-chloroform mixtures as well as spin coating 0.075% and 0.015% solutions. Excess solvent was removed by heating to 50 °C for 40 min under vacuum. Films of D7AOB [20] were prepared by spin coating its solutions in toluene at 5000 rpm for 30 s onto soda-lime glass plates at room temperature.

Nine-layer Langmuir-Blodgett films were prepared in a Teflon Lauda trough in a Class 100 clean room. The subphase was triply distilled water, on which a monolayer of 12-8(poly)diacetylene was deposited and allowed to spread before compressing with a movable barrier to a surface pressure of 30 mN/m. Glass microscope slides served as substrates, which were vertically dipped through the monolayer at a speed of 1 mm/min. This deposition resulted in a transfer ratio of ~0.96. Photopolymerization was induced by 40 min exposure to a Hg lamp uv source in a Class 100 clean room. Linear polarization of uv light was achieved with a polarizer sensitive to the Hg spectrum.

## V. RESULTS AND DISCUSSION

### A. Soda-lime glass substrate

Using x-ray reflectivity, we studied soda-lime glass as substrates for the work reported in this paper. X-ray specular reflections from bare glass substrates after chemical etching for 0, 5, 8, and 12 h are shown in Fig. 3. Because there was a single rough interface between air and glass, the specular reflections were fit to Eq. (3), from which the electron density of the glass and its surface

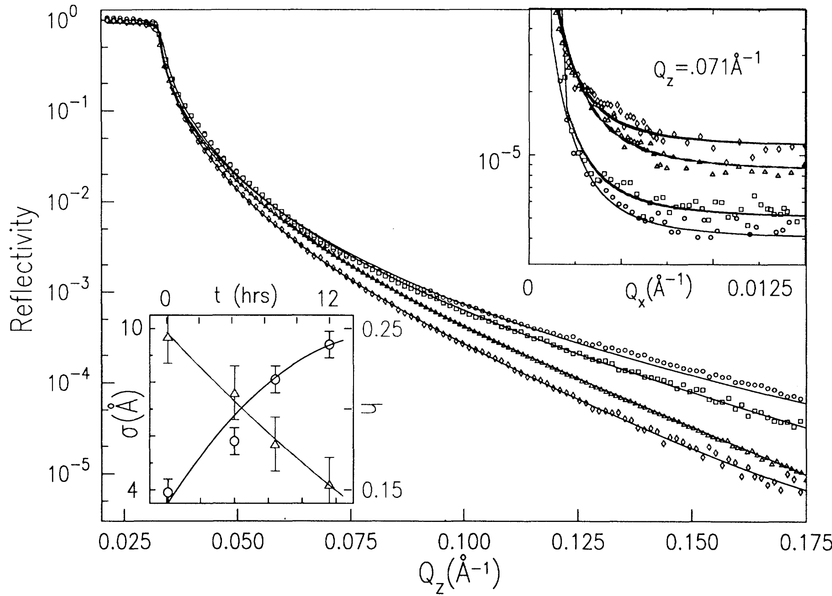


FIG. 3. Specular scans showing increase in falloff due to increasing roughness for KOH-roughened glass, with fit parameters given in text for (○) 0 h, (□) 5 h, (△) 8 h, and (◇) 12 h. Top inset shows diffuse wings of transverse scans of reflectivity, with corresponding increase in diffuse wings arising from increasing roughness. Symbols denote experimental data collected at $q_z$ = 0.0712 Å$^{-1}$ and solid lines best fits to the model described by Eq. (4). Lower inset plots simultaneously increasing rms roughness $\sigma$ and decreasing roughness exponent $h$ versus etch time.

roughness were accurately determined. The average electron density for a number of soda-lime glass surfaces was measured to be $\rho = (0.78 \pm 0.05)$ Å$^{-3}$, which was slightly larger than that of $SiO_2$, $\rho = (0.72 \pm 0.05)$ Å$^{-3}$. The value $\rho$ for soda-lime glass agreed well with the value calculated ($\rho_{calc}$ =0.741 Å$^{-3}$) from its chemical composition: (73±1)% $SiO_2$, (14±0.5)% $Na_2O$, (6.75±0.75)% CaO, (4.5±0.5)% MgO, and (1.5±0.5)% $Al_2O_3$ [21], with densities 2.32 g/cm$^3$, 2.27 g/cm$^3$, 3.25 g/cm$^3$, 3.58 g/cm$^3$, and 3.97 g/cm$^3$, respectively. Even though the difference in electron densities of soda-lime glass and $SiO_2$ is very small, it has nontrivial optical effects for x rays, as we will discuss in the next subsection. The rms values of the surface roughness from fits shown in Fig. 3 were determined to be 3.9±0.5 Å, 5.8±0.5 Å, 8.0±0.5 Å, and 9.4±0.5 Å, respectively, using a multiplicative Debye-Waller-like factor, and were found to increase monotonically with etch time as expected. The value of measured roughness was in agreement with the value observed using atomic force microscopy [22] over areas comparable with the coherence area of our x-ray beam.

Roughness in the plane of the substrate has been determined from analysis of transverse scans using a numerical adaptation of Eq. (4). Etching in KOH solution also allowed progressive roughening of the same surface so as to determine the effect on the "roughness exponent" $h$ of increasing etch time. The central (specular) peak and diffuse wings in the transverse curves in the Fig. 3 inset were fitted over the data ranging from the central maximum to the diffuse wings. The wings are shown normalized by the intensity of the incident beam (without vertical shift), illustrating directly the increase in diffuse scattering arising from increased roughness, with convolution of experimental data with arm-zero resolution function performed, and geometrical correction made for deviation of $q_z$ from the Bragg condition [9]. Analysis yielded the following results: (a) $\sigma$=3.9±0.5 Å, $\xi$=1275±30 Å, $h$=0.25±0.03, (b) $\sigma$=5.8 Å, $\xi$=1373 Å, $h$=0.21, (c) $\sigma$=8.1 Å, $\xi$=1301 Å, $h$=0.18, and (d) $\sigma$=9.4 Å, $\xi$=1254 Å, $h$=0.15 for $q_z$=0.0712 Å. Here, $\sigma$ is the rms roughness equivalent to the value obtained from longitudinal scans, $\xi$ is the roughness cutoff length, and $h$ is the exponent described earlier. The cutoff length for the roughness was essentially unchanged as it depended primarily on the resolution of the experimental setup, while exponent $h$ decreased as a function of etch time. The values obtained for $\sigma_{rms}$ from transverse-scan analysis matched those parameter values obtained from longitudinal scans within the experimental error.

### B. Thin conducting ITO film

Used in liquid crystal displays to apply an electric field across the cell and alter molecular orientation, ITO coating on glass is used because of its good electrical conductivity and optical transparency. A ~1200-Å-thick layer of $SiO_2$ is deposited [21] on the surface of glass by a full-immersion method to coat both its sides. ITO is then sputtered on one side to a thickness of ~300 Å. The $SiO_2$ between the ITO and glass prevents nullification of accumulated charge due to migration of ionic impurities (e.g., alkalis such as $Na^+$) from within the glass to the charged ITO surface. The disparity in thickness between the ITO and $SiO_2$ layers is due to the need to preserve the $SiO_2$ "barrier layer" after repeated chemical etchings used to "pattern" the ITO layer, e.g., in the production of flat panel displays.

The specular reflectivity curve of ITO coated glass [Fig. 4(a)] showed two superimposed periodicities with very different amplitudes, indicating the presence of two layers of different thickness and electron densities. There was no internal structure to these layers, hence only Kiessig fringes were observed. Fits of the reflectivity curve to

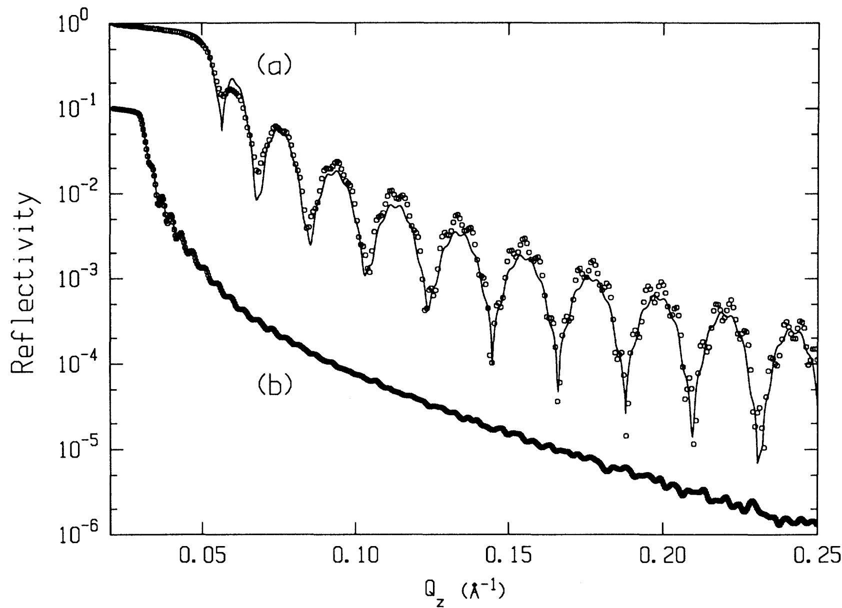


FIG. 4. Specular reflectivity scans showing two modulations arising from layers of ITO and $SiO_2$ on soda-lime glass. (a) ITO-$SiO_2$ of thickness 254 Å-1330 Å, line shows the fit discussed in the text. (b) Opposite side of same glass plate (without ITO) showing interference fringes from 1320 Å-thick $SiO_2$ layer. The solid curve in (b) is drawn as a guide to the eye.

Eq. (8) revealed an ITO film of thickness 254±1 Å and electron density $\rho$ of (1.90±0.06) $Å^{-3}$, and an $SiO_2$ thickness 1330±3 Å and $\rho$ of 0.72 $Å^{-3}$. We assumed that the film roughness was Gaussian. Interfacial roughness was then determined to be $\sigma_{\rm rms} = 3.64$ Å.

Small modulations in the reflectivity curve were also observed from an examination of the reverse side of the glass plate, indicated by the presence of an oxidation layer of thickness 1320 Å [Fig. 4(b)], laid down before deposition of ITO to prevent migration of Na ions to the surface when used in a liquid crystal device [23]. The difference in the critical scattering vector for the ITO-coated ($\sim 0.055$ $Å^{-1}$) side and $SiO_2$-coated ($\sim 0.03$ $Å^{-1}$) side of the glass plate is due to its dependence on the electron density, and these values yield film electron densities which match closely with the fitted results.

### C. Lecithin films

Lecithin is a well-known agent used to achieve homeotropic (perpendicular to the substrate) alignment of liquid crystal molecules [24]. Most studies to date have focused on the ordering and phase transitions induced in the liquid crystal material in contact with lecithin [25], rather than directly with the glass substrate. We discuss structure in spin-coated and dipped lecithin films as it relates to film thickness and the resulting appearance of Kiessig fringes and Bragg peaks in reflectivity data.

Samples were prepared by dipping the glass substrate in 0.2% and 2.0% solutions of lecithin in chloroform, and spin coating 0.015% and 0.075% lecithin-chloroform solutions at 3000 rpm for 30 s. As indicated by the x-ray reflectivity curves in Figs. 5(a,b), the two spin-coated films were relatively thin and exhibited Kiessig fringes near the first-order Bragg peak, and fits yielded overall film thicknesses of 96.5±1.3 Å and 301.1±1.3 Å, respectively, and layer spacings of 45.7±0.4 Å and 39.7±0.4

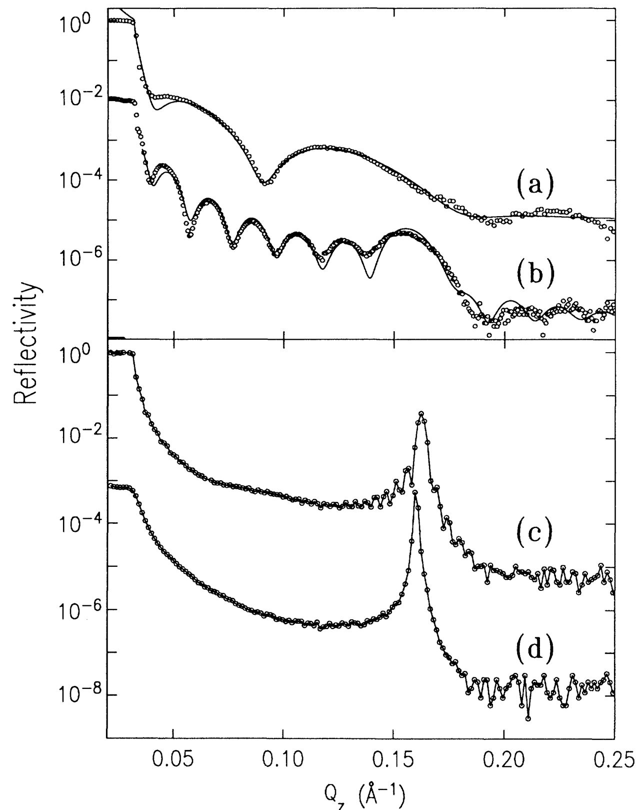


FIG. 5. Specular reflectivity for spin-coated and dipped thin films of egg lecithin–chloroform. (a) 0.015% and (b) 0.075% spin-coated lecithin films showing coherent summation of Bragg peaks and Kiessig fringes. Solid lines are fits to Eq. (10), symbols are experimental data. (c) 0.2% and (d) 2.0% dipped lecithin films showing Bragg peak with Kiessig fringes in thinner film, while thickness in thicker film exceeds beam coherence length in normal direction.

Å, corresponding to two and eight bilayers, respectively. These parameters were obtained from fits to Eq. (10). Lecithin is known [26] to stratify with a bilayer as the smallest repeat unit, with zwitterionic head groups facing each other and alkane tails extending outward. In these spin-coated films, fits to films of different thickness yielded integer numbers of bilayers with bilayer spacing calculated from the Bragg peak position.

The thicker, dipped films [Figs. 5(c,d)] exhibited a Bragg peak corresponding to a layer spacing of 38.8 Å and a noticeable reduction in intensity after the Bragg peak due to interference between x rays reflected from the two interfaces and diffracted from the internal layer structure. The Kiessig fringes near the Bragg peak for the 0.2% dipped film yielded a film thickness of 1280 Å. For the 2.0% dipped sample, the Bragg scattering was strong and sharp (peak intensity was 40% of incident beam intensity and full width at half maximum was 0.000 926 $Å^{-1}$), but no Kiessig fringes were observed. The strength and sharpness of the Bragg peak indicated the highest quality of the layered structure of lecithin films, while the absence of Kiessig fringes may be principally attributed to its large thickness, which exceeded 5000 Å as estimated from the Bragg peak width. Dipped lecithin films thicker than the 2.0% sample were prepared, but were less uniform as judged by sample mosaic width and Bragg peak intensity.

### D. Langmuir-Blodgett films

We probed structural anisotropy in Langmuir-Blodgett films, photopolymerized with linearly polarized uv light. Polymerized films of PDA are important due to their large nonlinear optical susceptibility [27]. No studies of the structural anisotropy in "linearly" polymerized LB films have been previously reported. Schadt *et al.* [28] used linearly polarized uv light to polymerize spin-coated poly(vinyl 4-methoxycinnamate) films to obtain homogeneous liquid crystal alignment. The technique of linear photopolymerization of alignment layers is being developed to replace the "rubbing" technique which results in static surface charge buildup detrimental to the thin-film transistor arrays on the substrate.

Monomer, isotropically polymerized, and linearly polymerized nine-layer Langmuir-Blodgett films of 12-8(poly)diacetylene were studied to determine the structural changes induced by polymerization and if/how they depended on the direction of polarization of the light used.

Longitudinal scans were performed with the sample in two orientations ($x$ and $y$), obtained by rotating the sample by 90° about the surface normal. The $x$ orientation was defined to be the one in which the direction of the $\vec{E}$ field of uv light, used in linear polymerization, was confined to the scattering plane. In the $y$ orientation, the direction of linear polymerization was pointing out of and perpendicular to the scattering plane. Before polymerization, both sample orientations yielded similar reflectivity curves [Fig. 6(a)] exhibiting poorly defined Kiessig fringes due to the lack of film uniformity. Upon polymerization with depolarized light the Kiessig fringes became equally well defined in the $x$ and $y$ orientations. The mosaic scans yielded somewhat wider peaks for two different orientations of the film than the monomer film, suggesting increased misorientation of the film, perhaps due to increased roughness (estimated from fits to be ~19.6 Å in the $y$ direction of the linearly polymerized film) or finite size effects.

However, upon linear polymerization, longitudinal scans in the $x$ orientation show Kiessig fringes that became more pronounced over the measured $q$ range, indicating that the overall film was better defined (more uniform) than the unpolymerized film [Fig. 6(b)]. Scans in the $y$ orientation, however, showed essentially monomer-like features. Insets in Fig. 6 show $\omega$ scans in the two orientations. The peak broadening in the $y$ direction in the polymerized film in (b) indicated partial breakup of layers in direction perpendicular to polarization direction. The reflectivity curves were fitted to Eq. (11) assuming an average electron density consisting of four bilayers and one monolayer for the nine-layer film, with crests in the electron density modulation representing head groups or double bonds, and the troughs allowing for low electron density regions [left inset, Fig. 6(a)]. The fits showed that the full-base width of the crests at the sites of the head groups and double bonds narrowed upon polymerization, while the bilayer thickness (55.7±0.4 Å for monomer samples in the $x$ and $y$ directions) increased by $\sim 1.5$ Å, which is in keeping with previously published results [29]. Monolayer thickness was found to remain essentially unchanged (27.0 Å). Average electron densities were 0.28 $Å^{-3}$ and 0.27 $Å^{-3}$ in both the directions parallel and perpendicular to the direction of polymerization, respectively, which agreed closely with values obtained from stoichiometric calculation.

Thus chemical bonding within the plane of the layers induced by photopolymerization served to "straighten" the layers, making the overall film more uniform in one direction. Morphological anisotropy (or formation of "ribbons") was the result of preferential $\pi$ bonding along the $\vec{E}$ field of linearly polarized light. This anisotropy was detectable due to an elongated coherence area of the x-ray beam. The two coherence lengths in the plane of the substrate are the longitudinal (in beam direction) and transverse (perpendicular to beam and scattering plane) lengths, which are $\sim 6000$ Å and $\sim 300$ Å, respectively. The elongated coherence area [30] allows for averaging over the surface weighted toward the incident beam direction by a factor of $\sim 20$:1. It makes it possible to determine morphological anisotropy arising from linear polymerization. In the $x$ orientation, the $\pi$ bonds are oriented along the longitudinal coherence length and thus a longer dimension is probed by x rays in the more uniform film direction. In the $y$ orientation, the $\pi$ bonds are at right angles to the longitudinal coherence length. Consequently, a longer dimension along the less uniform direction is probed. This difference is reflected in the differences of pronouncedness of the Kiessig fringes. In the $y$ orientation, one also observes broadening of the $\omega$ scans

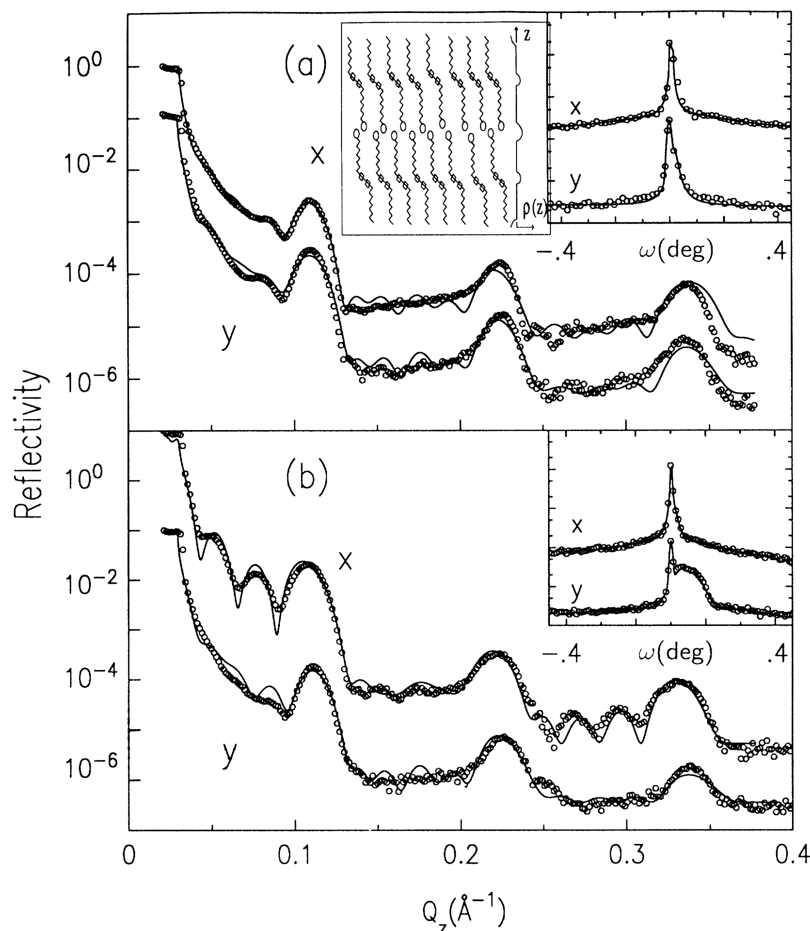


FIG. 6. Specular reflectivity scans for (a) monomer nine-layer PDA Langmuir-Blodgett films probed with x-ray beam direction in two orthogonal ($x$ and $y$) directions, and (b) after polymerization with the electric field of uv light in $x$ orientation, the Kiessig fringes developed very well in the $x$ orientation but the film structure remained monomerlike in the $y$ direction. Dotted lines represent theoretical fits to Eq. (11). Insets show the corresponding $\omega$ scans, which were practically unchanged in the $x$ direction while noticeably broadening in the $y$ direction, with lines drawn as guides to the eye. Left inset shows structure of bilayer with form of electron density modulation used to model results.

due to "finite size effects" (i.e., ordered regions smaller than the coherence length).

### E. Liquid crystal films: D7AOB

Liquid crystal thin films of D7AOB [20] were deposited by spin coating on soda-lime glass to study the interaction between liquid crystals and solid surfaces as a function of temperature and film thickness. At specific spin rate, spin duration, and substrate temperature, the amount of liquid crystal molecules deposited was determined by the concentration of its solution in toluene. We studied a series of samples which were prepared in concentrations from 0.5 to 50 wt % solution and obtained coherent and incoherent summations of Bragg peaks and Kiessig fringes based on film morphology over the beam coherence area.

The most uniform and stable liquid crystal film was obtained when 5% solution was used. A longitudinal scan along the surface normal is shown in Fig. 7(a) in the smectic phase at 37.6 °C for D7AOB. The interference between the Fresnel reflection and Bragg scattering, as demonstrated by enhancement and extinction of scattered intensity above and below the first-order Bragg peak ($q_z = 0.216$ Å$^{-1}$), the sharpness of the Bragg peak in $\omega$ scans, and the Kiessig fringes extending over a wide $q$ range indicated that this liquid crystal film was highly uniform and near perfectly parallel to the substrate surface. The smectic layer spacing measured from the position of the Bragg peak was 29.40±0.05 Å, in good agreement with the D7AOB molecular length. The thickness of this film determined from the period of the Kiessig fringes was 1200±10 Å, which was consistent with the value evaluated from the width of the Bragg peak.

The x-ray reflectivity profile from the D7AOB film prepared at low concentration (0.5%) is shown in Fig. 7(b). The wide period of Kiessig fringes gave a value of 37 Å corresponding to two layers in the crystalline phase of D7AOB. The positions and widths of the Bragg peaks in this sample were not substantially different from the 5% sample. The peak intensity was about ten times lower and agreed with our expectations as about ten times less material was deposited on the substrate. The adsorbed bilayer had been observed in all samples, but the Kiessig fringes produced by this bilayer became more obscure with increasing concentration as it was buried under more material. The amount of D7AOB deposited could also be evaluated from the integrated intensities of the Bragg peaks. Morphology of these films was found to be consistent with the Stranski-Krastanov growth mode [31],

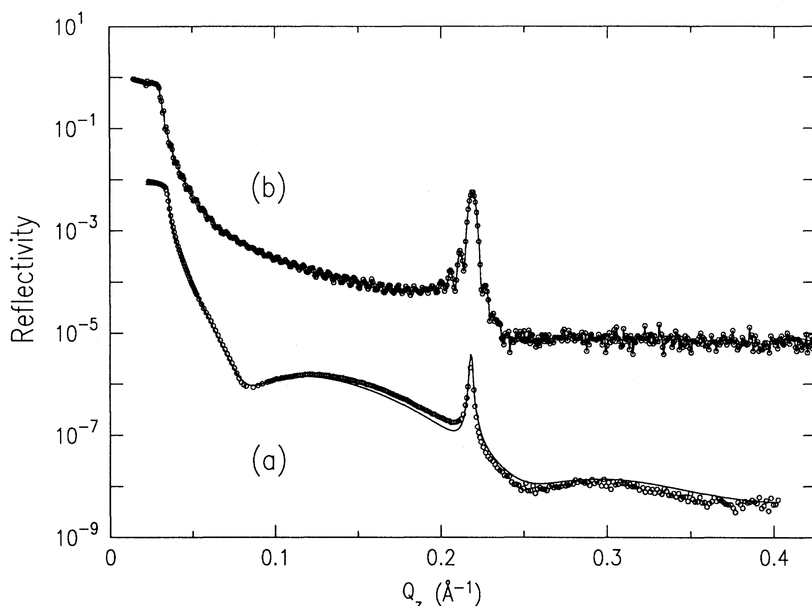


FIG. 7. (a) Specular reflectivity of 0.5% D7AOB film on bare glass showing smectic-*A* peak superimposed on broad Kiessig fringe corresponding to 37 Å thickness of adsorbed layer. Line is a fit to scattering modeled as incoherent contributions from the adsorbed layer and the overall film. (b) Specular reflectivity of 1200 Å-thick 5% D7AOB film on bare glass in the smectic-*A* phase at 37.6 °C. Bragg peak position corresponds to layer spacing of 29.40 Å, and the fine Kiessig fringes and destructive falloff after peak position indicate overall film uniformity. Line is drawn as guide to the eye.

commonly observed in epitaxial growth of semiconductor materials. It involves a uniform layer adsorbed on the surface with three-dimensional clusters on top of it. The fit shown in Fig. 7(b) for this morphology was based on a model involving the incoherent summation of the broad Kiessig fringes from the adsorbed layer and the Bragg peak as discussed in Ref. [20].

The liquid crystal islands on top of the adsorbed layer of D7AOB in the 0.5% sample exhibited all of the bulk phase transitions, i.e., crystalline to smectic *A* (Sm-*A*) at 34 °C, Sm-*A* to nematic at 54.5 °C, and nematic to isotropic at 71 °C. The Kiessig fringes corresponding to the adsorbed layer became less pronounced only above the nematic-isotropic transition temperature ($T_{NI}$) and eventually disappeared at 102 °C (more than 30 °C above $T_{NI}$) without substantial change in its thickness. This adsorbed layer was recovered as the temperature was later lowered. Its persistence suggested strong interaction between the liquid crystal molecules and the substrate. Clark [32] reported similar phenomena which he termed the "surface memory effect." We believe that this adsorbed, highly ordered layer is the cause of the surface memory effect observed for the bare glass surface.

## VI. CONCLUSIONS

In summary, we have demonstrated the power of x-ray reflectivity technique in characterizing the surface roughness of thin organic and metallic films and determining their electron densities and morphology. We discovered several interesting phenomena in these films which are of technological importance. The rms roughness $\sigma$ and height-height correlations for KOH-etched soda-lime glass were characterized, which showed increased rms and lateral roughness as well as diffuse scattering upon increasing etch time. The structure of thin ($\leq$ 300 Å) and thick ($\geq$ 1000 Å) lecithin films deposited on soda-lime glass was determined, in which the coherent summation of Bragg peaks and Kiessig fringes yielded an integer number of bilayers in these thin films. Spin-coated D7AOB films exhibited Stranski-Krastanov-like growth mode upon initial growth from solution. A thin adsorbed layer was found to be the likely source of surface memory effect as it persisted $\sim$30 °C beyond the bulk clearing temperature. We also discovered an effect, namely, the structural anisotropy in Langmuir-Blodgett deposited 12-8 (poly)diacetylene induced by linear polymerization, which is probed by making use of the elongated nature of the in-plane x-ray coherence area.


## ACKNOWLEDGMENTS

We gratefully acknowledge the help, in various forms, of V. Surendranath, S. Sabol-Keast, C. Rosenblatt, D. Fredley, H. Vithana, D. Johnson, M. Groom, P. Dunn, and J. West during this work. This research was supported by NSF Science and Technology Center, ALCOM, Grant No. DMR-89-20147.



[1] M. Barmentlo, Ph.D. thesis, Philips Research Laboratories, Netherlands, 1993.

[2] N. G. Cave, R. A. Cayless, L. B. Hazell, and A. J. Kinloch, Langmuir **6**, 529 (1990).

[3] R. M. Overney, E. Meyer, J. Frommer, H.-J. Guntherodt, G. Decher, J. Reibel, and V. Sohling, Langmuir **9**, 341 (1993).

[4] W. Lesslauer, Acta Crystallogr. Sect. B **30**, 1927 (1974).

[5] J. Als-Nielsen, in *Structure and Dynamics of Surfaces II*, edited by W. Schommers and P. von Blanckenhagen (Springer-Verlag, Berlin, 1987), p. 181; P. Lambooy, Ph.D. thesis, University of Amsterdam, Netherlands, 1992.

[6] R. M. Richardson and S. J. Roser, Liq. Cryst. **2**, 797 (1987).

[7] P. S. Pershan, A. Braslau, A. H. Weiss, and J. Als-Nielsen, Phys. Rev. A **35**, 4800 (1987).

[8] Robert Holyst, Douglas J. Tweet, and Larry B. Sorensen, Phys. Rev. Lett. **65**, 2153 (1990).

[9] D. E. Savage, J. Kleiner, N. Schimke, Y.-H. Phang, T. Jankowski, J. Jacobs, R. Kariotis, and M. G. Lagally, J. Appl. Phys. **69**, 1411 (1991).

[10] B. E. Warren, *X-ray Diffraction* (Dover Publications, New York, 1969).

[11] B. D. Cullity, *Elements of X-ray Diffraction* (Addison-Wesley, Reading, MA, 1956).

[12] R. James, *The Optical Principles of the Diffraction of X-rays* (G. Bell and Sons Ltd., London, 1948).

[13] M. Born and E. Wolf, *Principles of Optics*, 6th ed. (Pergamon, New York, 1980).

[14] B. B. Mandelbrodt, *The Fractal Geometry of Nature* (Freeman, New York, 1982).

[15] S. K. Sinha, E. B. Sirota, S. Garoff, and H. B. Stanley, Phys. Rev. B **38**, 2297 (1988).

[16] R. E. Geer, R. Shashidar, A. F. Thibodeaux, and R. S. Duran, Phys. Rev. Lett. **71**, 1391 (1993).

[17] H. Kiessig, Ann. Phys. (Leipzig) **10**, 769 (1931).

[18] J. J. Benattar, J. Daillant, L. Bosio, and L. Lager, J. Phys. Colloq. (Paris) **C7**, 39 (1989); A. Leuthe and H. Riegler, J. Phys. D **25**, 1786 (1992).

[19] F. Rieutord, J. Benattar, L. Bosio, P. Robin, C. Blot, and R. de Kouchkovsky, J. Phys. (Paris) **48**, 679 (1987).

[20] Yushan Shi, Brian Cull, and Satyendra Kumar, Phys. Rev. Lett. **71**, 2773 (1993).

[21] Cindy Imminik, Donnally technical representative (private communication).

[22] H. Vithana (private communication).

[23] D. J. Channin and A. Sussman, in *Display Devices*, edited by J. I. Pankove, *Topics in Applied Physics*, Vol. 40, (Springer-Verlag, Berlin, 1980).

[24] J. Cognard, Mol. Cryst. Liq. Cryst. **78**, Suppl. 1, 1 (1982).

[25] K. Flatischler, L. Komitov, S. T. Lagerwall, B. Stebler, and A. Strigazzi, Mol. Cryst. Liq. Cryst. **198**, 119 (1991).

[26] D. M. Small, J. Lipid Res. **8**, 551 (1967); V. Luzzati, J. Mol. Biol. **45**, 355 (1972).

[27] G. Carter, J. Hyniewicz, M. Thokur, Y. Chen, and S. Meyler, Appl. Phys. Lett. **49**, 998 (1986); K. Ogawa, N. Mino, H. Tamina, and N. Sonoda, Langmuir **5**, 1415 (1989).

[28] M. Schadt, K. Schmitt, V. Kozinkov, and V. Chigrinov, Jpn. J. Appl. Phys. **31**, 2155 (1992); M. Schadt, Liq. Cryst. **14**, 73 (1993).

[29] G. Wegner, Pure and Appl. Chem. **49**, 443 (1977).

[30] T. P. Russell, Mater. Sci. Rep. **5**, 171 (1990).

[31] J. A. Venables, G. D. T. Spiller, and M. Hanbucken, Rep. Prog. Phys. **47**, 399 (1984).

[32] N. A. Clark, Phys. Rev. Lett. **55**, 292 (1985).